Analysis of Aquaporin-Mediated Diffusional Water Permeability by Coherent Anti-Stokes Raman Scattering Microscopy

Keiji Ibata,[†△] Shinichi Takimoto,[‡△] Toshinori Morisaku,[§] Atsushi Miyawaki,[†*] and Masato Yasui[§*]
[†]Laboratory for Cell Function Dynamics, Brain Science Institute, The Institute of Physical and Chemical Research (RIKEN), Saitama, Japan; [‡]Medical Technology R&D Division, Olympus Corporation, Tokyo, Japan; and [§]Department of Pharmacology, School of Medicine, Keio University, Tokyo, Japan

ABSTRACT Water can pass through biological membranes via two pathways: simple diffusion through the lipid bilayer, or water-selective facilitated diffusion through aquaporins (AQPs). Although AQPs play an important role in osmotic water permeability (P_f), the role of AQPs in diffusional water permeability remains unclear because of the difficulty of measuring diffusional water permeability (P_d). Here, we report an accurate and instantaneous method for measuring the P_d of a single HeLa S3 cell using coherent anti-Stokes Raman scattering (CARS) microscopy with a quick perfusion device for H_2O/D_2O exchange. Ultra-high-speed line-scan CARS images were obtained every 0.488 ms. The average decay time constant of CARS intensities (τ_{CARS}) for the external solution H_2O/D_2O exchange was 16.1 ms, whereas the intracellular H_2O/D_2O exchange was 100.7 $\pm$ 19.6 ms. To evaluate the roles of AQP in diffusional water permeability, AQP4 fused with enhanced green fluorescent protein (AQP4-EGFP) was transiently expressed in HeLa S3 cells. The average τ_{CARS} for the intracellular H_2O/D_2O exchange in the AQP4-EGFP-HeLa S3 cells was 43.1 $\pm$ 15.8 ms. We also assessed the cell volume and the cell surface area to calculate P_d. The average P_d values for the AQP4-EGFP-HeLa S3 cells and the control EGFP-HeLa S3 cells were 2.7 $\pm$ 1.0 $\times$ 10^{-3} and 8.3 $\pm$ 2.6 $\times$ 10^{-4} cm/s, respectively. AQP4-mediated water diffusion was independent of the temperature but was dependent on the expression level of the protein at the plasma membrane. These results suggest the possibility of using CARS imaging to investigate the hydrodynamics of single mammalian cells as well as the regulation of AQPs.

INTRODUCTION

The movement of water across cell membranes has been a topic of active research for more than a hundred years. The cell plasma membrane is largely composed of phospholipid bilayers, and water can cross the cell membranes via two basic pathways: simple diffusion through the lipid bilayer or transit through water-selective channels, i.e., facilitated diffusion (1). Diffusional water permeability (P_d) is defined as the flux of radioactively labeled water moving across a membrane under an isotopic gradient of water. The diffusion of water is temperature-dependent and is constrained by membrane lipid organization and fluidity; therefore, it has a high Arrhenius activation energy (Ea >10 kcal/mol) (2,3). On the other hand, osmotic water permeability (P_f) reflects membrane water permeability under the condition of osmotic gradients that constitute a driving force for water flow. Osmotic water permeability is therefore relevant to cell volume regulation and epithelial secretion or absorption.

Aquaporin (AQP) is a membrane channel protein that is selectively permeated by water. AQPs have been shown to increase the osmotic water permeability of membranes (3). There are 13 members of the AQP family in humans (4), and some of them, such as AQP2 in nephrogenic diabetes insipidus (5) and AQP0 in cataracts (6), have been shown to have clinical relevance. The atomic structure of human AQP1 has revealed the molecular mechanisms responsible for the selectivity of AQP pores for water (7). Molecular dynamics simulations have also demonstrated how water molecules pass through AQP pores (8). Although AQPs increase the P_f of cell membranes under osmotic gradients, the extent to which AQPs contribute to the P_d under isotonic conditions has not been well defined because of the difficulty of performing such measurements.

The P_f can be assessed by measuring the rate of cell volume changes under osmotic stress in single mammalian cells or oocytes (9). Several methods have been used to measure the P_d of cell membranes. NMR can measure the exchange rate of intracellular/extracellular water in tissues or cells, although signals from single cells cannot be separated (10–13). Kuwahara et al. developed a fluorescent probe, the fluorescence of which increases when the intracellular H_2O is replaced with D_2O (14). Consequently, water movements can be measured by monitoring the fluorescence intensity in the cells. Potma et al. used a coherent anti-Stokes Raman scattering (CARS) laser-scanning microscope to image the intracellular hydrodynamics in single living cells (15). A unique signal can be detected from both excited O-H vibrations in H_2O and excited O-D vibrations in D_2O. The authors observed the intracellular hydrodynamics in a single microorganism, *D. discoideum*, by exchanging extracellular H_2O with D_2O. According to their article, the P_d of *D. discoideum* is 2.2 $\times$ 10^{-4} cm/s, which is smaller than that of mammalian cells such as erythrocytes.

Submitted April 26, 2011, and accepted for publication August 26, 2011.

△Keiji Ibata and Shinichi Takimoto contributed equally to this work.

*Correspondence: myasui@sc.itc.keio.ac.jp or matsushi@brain.riken.jp

Editor: Levi A. Gheber.

0006-3495/11/11/2277/7 $2.00

doi: 10.1016/j.bpj.2011.08.045

Here, we report an advanced experimental technique for accurately measuring the P_d of the plasma membrane of single mammalian cells based on CARS microscopy and using a quick perfusion device for H_2O/D_2O exchange. Our line-scan imaging protocol for monitoring the intracellular H_2O/D_2O exchange has a sufficiently high temporal and spatial resolution to distinguish AQP4-mediated diffusion from simple diffusion through the lipid bilayer of the cell membrane. As expected, AQP4-mediated water diffusion is temperature-independent but dependent on the expression level of the protein at the plasma membrane of the cells.

MATERIALS AND METHODS

CARS microscopy

Our microscope device used to visualize the water dynamics is shown in Fig. 1 *A*. We used a high-repetition-rate (76 MHz) pulsed laser source for CARS to ensure a signal/noise ratio sufficient to detect fast water dynamics in cells. As a laser source, a mode-locked Nd:YVO_4 laser (1064 nm, 7 ps, 76 MHz repetition rate; picoTRAIN Green & UV, IC-532-4000, High-Q, Rankweil, Austria) was used. A frequency-doubled 532-nm beam was used to pump an optical parametric oscillator (OPO) (Levante Emerald, AP&E, GmbH, Berlin, Germany). The output wavelength has a broad wavelength tuning range, 690–990 nm. To generate a CARS signal from a sample, the fundamental 1064 nm and the signal output from the OPO were used as a Stokes and a pump beam, respectively. Both beams were coupled and collinearly introduced into an Olympus laser scanning microscope (FV1000/IX81, Olympus, Tokyo, Japan) and focused onto a sample using an objective lens (UPlanSapo 60×W NA1.2/UIS2, Olympus). To further increase the throughput in the near-infrared (IR) wavelength region of our CARS microscope, a special near-IR coating was applied to the microscope system and the objective lens. The guiding optics included an afocal pupil-projection optical system (for a detailed description of this system, see Cheng et al. (16)). This also allowed us to easily compensate for chromatic aberrations and beam walk caused by the tuning of the signal wavelength. For CARS imaging, a forward-CARS signal was corrected using a condensing lens (IX2-LWUCD, NA0.55; Olympus) and a custom-built forward detector dedicated for use with an Olympus inverted microscope (IX-81).

For single-photon fluorescence imaging, an argon laser (488 nm) was used as an excitation laser. All the fluorescence images were obtained using the same microscope system. The confocal detector (photomultiplier tube (PMT)) in the scanner was used as a fluorescence-signal detector. A dichroic mirror inside the scanner was specially designed to enable the CARS and fluorescence signals to be obtained using the same filter setup.

Rapid exchange of buffer solution

The balanced salt solution (BSS) used during the imaging contained (in mM) 130 NaCl, 5.4 KCl, 2 $CaCl_2$, 1 $MgCl_2$, 10 HEPES, and 10 D-(+)-glucose (pH 7.4). The quick exchange of H_2O buffer with D_2O buffer was achieved using a stainless steel pipette 0.51 mm in diameter attached to a micromanipulator (Narishige, Tokyo, Japan) built on the microscope stage. The stainless steel pipette was set at a 45° angle relative to the stage and connected with a Teflon tube from a syringe pump (Harvard Apparatus, Holliston, MA). For each experiment, the culture medium was replaced with 5~10 μl of H_2O/BSS. Then, the external H_2O/BSS was replaced with 30 μl of D_2O/BSS by quickly flushing with a pipette placed 1~2 mm away from the cell (Fig. 1 *B*, *a*). Because of the limited volumes of the solutions, the external H_2O/BSS was quickly replaced by the D_2O/BSS. For the temperature experiments, the microscope lens and the stainless steel pipette were adjusted to the appropriate temperatures.

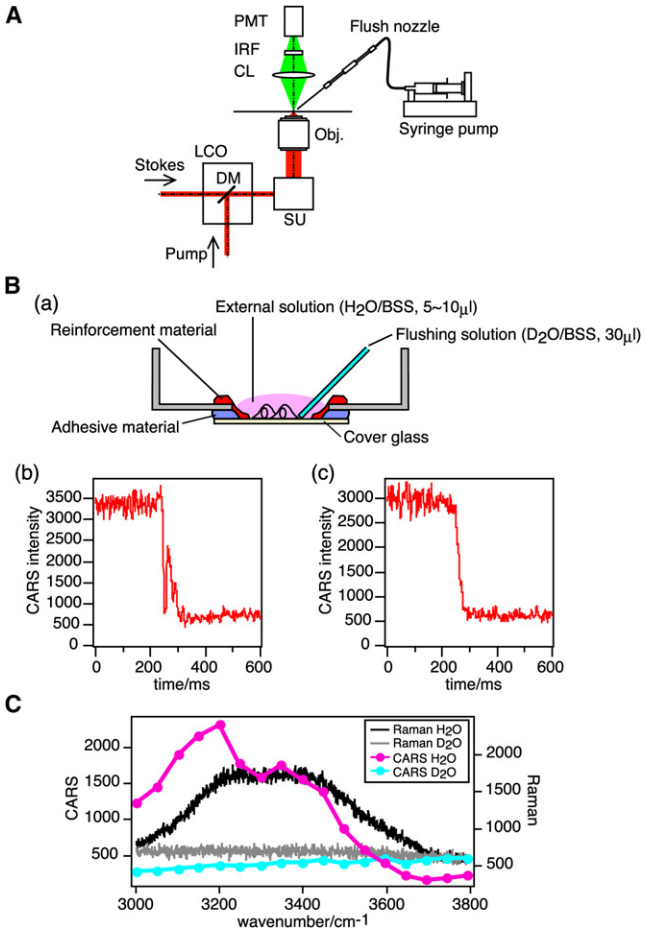

FIGURE 1 CARS microscopy with the rapid exchange of H_2O/D_2O. (*A*) Schema of CARS microscope. PMT, photomultiplier tube; LCO, laser coupling optics, including an afocal pupil-projection optical system; SU, scan unit; Obj., objective lens; DM, dichroic mirror; IRF, infrared cut filter; CL, condenser lens. (*B*, *a–c*) Schema of a glass-bottomed dish whose coverglass was reinforced (*a*), accompanied by intensity profiles of CARS signals during D_2O flushing into a dish without (*b*) and with (*c*) reinforcement. (*C*) Spectrum separation of H_2O from D_2O by Raman as well as CARS. CARS intensities were obtained with 3000–3800 cm^{-1} contrasts.

Culture dishes

To avoid defocusing while flushing the solution, the rim of the hollow in the glass-bottomed dish (Matsunami, Tokyo, Japan) was reinforced with a low elastic coefficient adhesive material. This reinforcement efficiently prevented defocusing caused by the replacement of the external solution (Fig. 1 *B*, *b* and *c*).

Cell culture and transfection

HeLa S3 cells were cultured on a reinforced glass-bottomed dish in Dulbecco's modified Eagle's medium containing 10% fetal bovine serum at 37°C in 5% CO_2. The transfection of plasmids, pEGFPN1-AQP4M23 or pEGFPN1 into HeLa S3 cells was performed using Lipofectamine LTX reagent (Invitrogen, Carlsbad, CA) according to the manufacturer's instructions. Two days after transfection, the culture dishes were examined to identify transfected cells expressing enhanced green fluorescent protein (EGFP). The transfected cells were then used for CARS imaging.

Estimation of cell volume and cell surface area

HeLa S3 cells were transfected with a plasmid carrying EGFP. Transfected HeLa S3 cells were imaged using 0.5-μm z-stack increments. The average cell volume and cell surface area were calculated using Volocity software (PerkinElmer, Waltham, MA).

CARS imaging and data analysis

Before starting the experiment, the CARS image was set to show a high intensity by adjusting the PMT. Images were captured at 35 ms/frame for xy images and 0.488 ms/line for line-scan images. For a single experiment, baseline images were acquired for 3 s, then D_2O/BSS was quickly applied using a syringe pump. Images were captured until the CARS intensities inside the cell reached a plateau. The laser intensities used in this measurement were ~100 mW for pump and 50 mW for Stokes before a microscope objective lens. With these laser intensities, we did not observe any morphological changes of HeLa S3 cells caused by photodamage during the measurements. A calibration curve of the CARS intensity for water was taken at different water concentrations. By means of our microscope-setup-tuned pump beam, at 793.7 nm, the CARS signal was detected from 0 to 100% H_2O/D_2O with 10% increments. The CARS signal intensities showed a nonlinear dependence for H_2O/D_2O concentration changes arising from the intrinsic characteristics of the CARS process (16). With our setup, we found that the CARS intensity is proportional to the numerical value of the water concentration to the 1.46th. Theoretically, the CARS signal intensity is expected to show a square dependence on water. In practice, however, we found that the CARS signal deviated from square dependence in the region of low water concentration. This deviation was considered to be a result of an inherent nonresonant background signal that may overshadow weak signals of interest (16). The decay time constant of the CARS signals (τ_{CARS}) was analyzed using IgorPro software (WaveMetrics, Portland, OR). Because the experimental results fit as a single-exponential decay, we were able to calculate the time constant of the H_2O efflux (τ_{H2O}) by multiplying τ_{CARS} with 1.46 to directly translate τ_{CARS} to τ_{H2O}. From τ_{H2O}, we calculated the rate constant k ($k = 1/\tau_{H2O}$). As a final step, each diffusional water permeability time constant (P_d) was calculated from each cell volume, surface area, and rate constant by applying the equation $P_d = 1/(k(S/V))$.

RESULTS

Imaging H_2O using CARS microscopy

Fig. 1 *C* shows the CARS spectra of water (H_2O) and deuterated water (D_2O) in the region between 3000 and 3800 cm^{-1}. In this region, a resonant CARS signal from the OH-stretch vibration of H_2O was obtained, consistent with the Raman spectrum of water (H_2O). On the other hand, no resonant CARS signal from the OD-stretch vibration of D_2O was observed, since the OD-stretch vibration of D_2O exists in the region between 2500 and 2800 cm^{-1} because of the isotope effect. The line shapes of these two CARS spectra did not completely match with those of Raman spectra due to a nonresonant background signal in the CARS process (16). The contrast in the CARS intensity between H_2O and D_2O was maximized when the signal wavelength was tuned to 793.7 nm (corresponding to 3200 cm^{-1}), allowing us to image the distribution and concentration of H_2O in a living mammalian cell using CARS microscopy in combination with the rapid exchange of H_2O/D_2O.

Imaging single HeLa S3 cells

Two-dimensional images were obtained at a very fast rate (35 ms/frame). Fig. 2 *A* shows two-dimensional images obtained every 35 ms after the flushing of D_2O/BSS (also see the Supporting Material movie). The external solution was replaced first, followed by replacement of the intracellular solution. We used a line-scanning mode of the microscope (FV1000/IX81) in which H_2O/D_2O exchange was measured with time resolution (0.488 ms/line (Fig. 2 *B*)). Fig. 2 *C* shows an example of line-scan intensity profiles. We used the decay time constant of the CARS signal (τ_{CARS}) as a time constant for H_2O/D_2O exchange. The τ_{CARS} for the external solution H_2O/D_2O exchange was 11.1 ms, whereas that for the intracellular H_2O/D_2O exchange was 123.7 ms. These data suggest that line-scan imaging using CARS microscopy with quick perfusion is suitable for studying the hydrodynamics of single HeLa S3 cells.

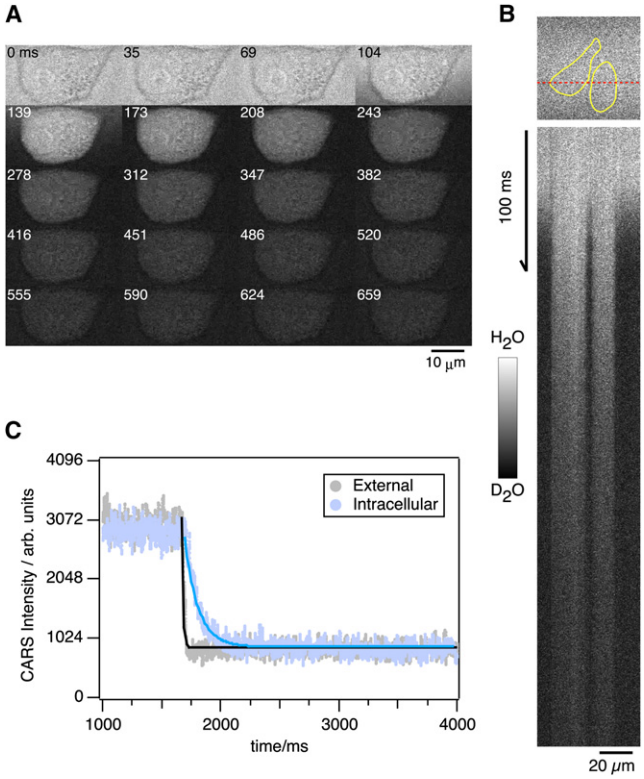

FIGURE 2 Time-lapse imagings of hydrodynamics in HeLa S3 cells during the exchange of H_2O/D_2O (O-H mode of CARS). (*A*) Sequential 2D images of hydrodynamics of HeLa S3 cells. H_2O/D_2O exchange was performed immediately after the third image was acquired. Scale bar, 10 μm. (*B*)_ Line-scan CARS image of HeLa S3 cells over the region indicated by the red dotted line in the upper image. The yellow lines indicate the cell boundaries. Scale bars, 20 μm and 100 ms. (*C*) Quantification of CARS intensities for inside (*blue*) and outside (*gray*) of HeLa S3 cell. The lines indicate the exponential curve fit.

Cell volume and cell surface

Both cell volume and cell surface area are considered important factors for the diffusion of water through cell membranes; the P_d can be increased when a cell has a larger surface area/volume ratio. To examine the relationship between the time constant measured using CARS microscopy and cell morphology, we assessed cell volume, surface area, and τ_{CARS} in single EGFP-transfected HeLa S3 cells (Fig. 3 *A*). The average cell volume was 4444 ± 1772 μm^3, and the average cell surface area was 3903 ± 1579 μm^2. The average τ_{CARS} for intracellular H_2O/D_2O transport was 100.7 ± 19.6 ms (average of 30 cells). Neither cell volume nor cell surface area was correlated with τ_{CARS} (Fig. 3, *B* and *C*), and there was no significant correlation between the surface area/cell volume (*S*/*V*) and the water exchange efficiency (Fig. 3 *D*). We next calculated the P_d based on the surface area, volume, and time constant (17). In our study, the calculated P_d for EGFP-transfected cells was 8.3 ± 2.6 × 10^{-4} cm/s.

Imaging of AQP4-transfected HeLa S3 cells

AQP is a water-selected channel protein that can facilitate water permeation across the plasma membranes of cells (9). To evaluate whether our CARS microscope setup could discriminate between water permeation in AQP-transfected cells and that in nontransfected HeLa S3 cells, we obtained images of the hydrodynamics of AQP4-transfected HeLa S3 cells. We transfected a plasmid-containing, EGFP-tagged AQP4 (AQP4-EGFP) or EGFP alone into HeLa S3 cells. After two days of transfection, AQP4-EGFP was efficiently expressed and transported to the plasma membrane (Fig. 4 *A*, *right*).

Having confirmed the surface expression of AQP4-EGFP, we next examined whether AQP4 alters diffusional water

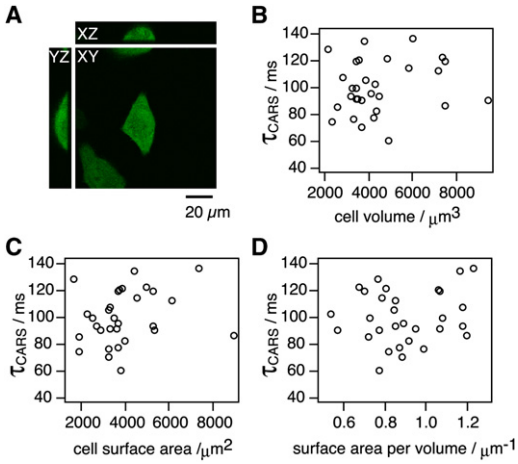

FIGURE 3 Relationships between cell morphology and diffusion time constant. (*A*) HeLa S3 cells expressing EGFP were imaged and analyzed using Volocity software. Orthogonal views through a single EGFP-HeLa S3 cell are shown. Scale bar, 20 μm. (*B–D*) Scattered plots of cell volume (*B*), cell surface area (*C*), and surface/volume ratio (*D*) with time constant, for 30 cells.

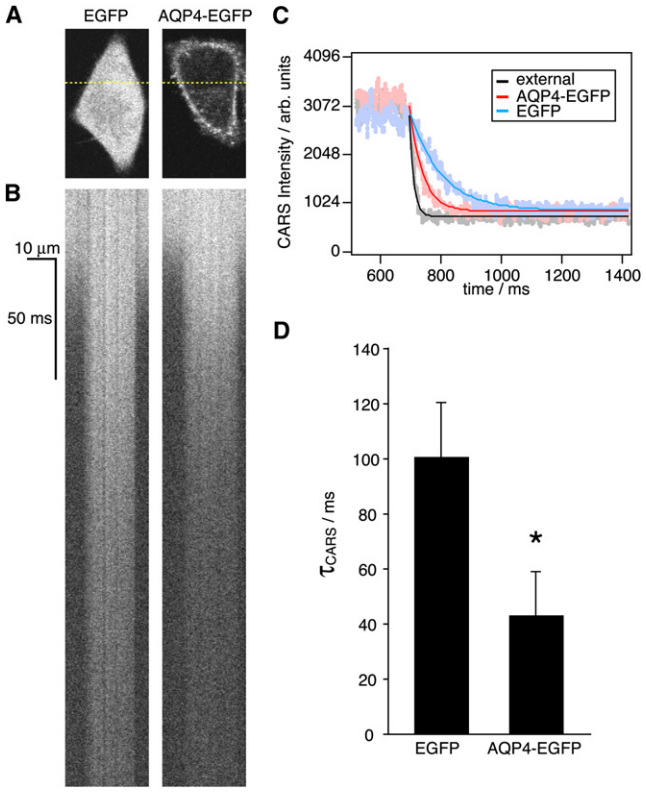

FIGURE 4 Comparison of membrane water permeability between EGFP- and AQP4-EGFP-transfected HeLa S3 cells. (*A*) Expression of EGFP or AQP4-EGFP proteins in HeLa S3 cells transfected with either EGFP control (pEGFPN1) or AQP4-EGFP plasmid (pEGFPN1-AQP4). A single slice is shown. (*B*) Line-scan CARS images of yellow dotted line of each HeLa S3 cells from *A*. Scale bars, 10 μm and 50 ms. (*C*) The CARS intensities for control EGFP-HeLa S3 cells (*blue*), AQP4-EGFP-HeLa S3 cells (*red*), and external region (*black*). (*D*) Averaged τ_{CARS} for control EGFP and AQP4-EGFP HeLa S3 cells. Statistical significance, $*p = 1.8 \times 10^{-16}$.

permeability. The average τ_{CARS} for the intracellular H_2O/D_2O exchange in AQP4-EGFP-HeLa S3 cells was 43.1 ± 15.8 ms (average of 25 cells), significantly lower than that in control EGFP-HeLa S3 cells (Fig. 4, *B–D*). The P_d for AQP4-EGFP-HeLa S3 cells was 2.7 ± 1.0 × 10^{-3} cm/s, much higher than that for the control EGFP-HeLa S3 cells (8.3 ± 2.6 × 10^{-4} cm/s). These results suggest that our CARS imaging method can reliably distinguish between two different hydrodynamics: AQP-mediated facilitated diffusion and simple diffusion through a lipid bilayer. Note that the expression levels of AQP4-EGFP at the cell surface, as revealed by the cell-surface fluorescence intensity (Fig. 5 *A*), was correlated with the P_d, suggesting that the amount of AQP4 on the cell surface strongly affected the efficacy of the hydrodynamics (Fig. 5 *B*).

Temperature dependency of hydrodynamics

The activation energy for AQP-mediated water transport is much lower than that for the simple diffusion of water

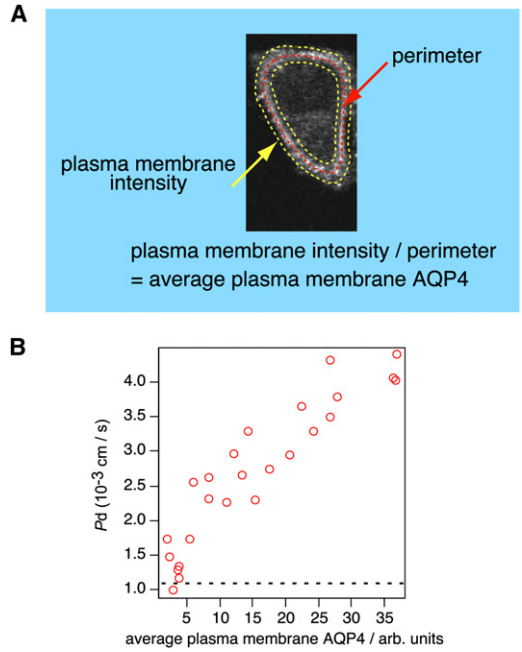

FIGURE 5 Correlation between expression levels of AQP4-EGFP and P_d. (*A*) Quantifying the average expression of AQP4-EGFP at plasma membranes. The EGFP fluorescence intensity is divided by the perimeter of the cell. (*B*) Plots of average plasma membrane AQP4-EGFP intensity and P_d for the 25 cells imaged and plotted. The dotted line indicates the average P_d for the control obtained in Fig. 3. The Pearson's correlation coefficient and the p value from a Spearman's rank test were $r = 0.92$ and $p = 0.0000015$, respectively.

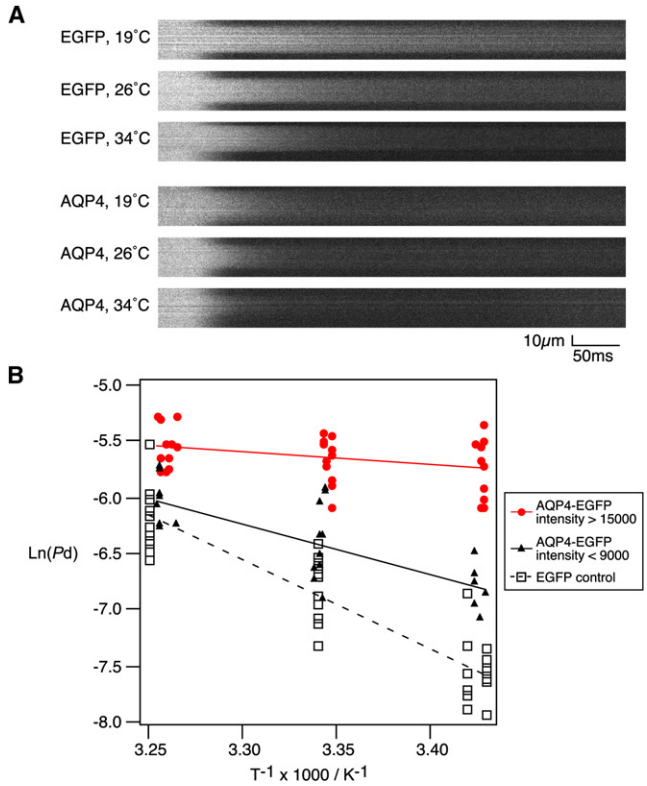

FIGURE 6 Temperature dependency for water permeation of EGFP- or AQP4-EGFP-transfected HeLa S3 cells. (*A*) Representative line-scan CARS images of EGFP- or AQP4-EGFP-transfected HeLa S3 cells at different temperatures. Scale bars, 10 μm and 50 ms. (*B*) Arrhenius plots for control, and for strong (intensity >15,000) and weak (intensity <9000) AQP4-EGFP-expressing HeLa S3 cells. The measured temperatures and P_d were converted for the Arrhenius plots. The activation energy was calculated from the slope of the line fit. For the control (*squares*), 16, 13, and 11 cells were imaged at temperature settings of 19, 26, and 34°C, respectively. For strong AQP4-expressing cells (*red circles*), 10, 11, and 11 cells were imaged at each temperature setting. For weak AQP4-expressing cells (*black triangles*), 7, 10, and 9 cells were imaged at each temperature.

through a lipid bilayer (17,18). To examine the activation energy of H_2O/D_2O exchange across cell membranes, we obtained CARS images at three different temperatures (~19°C, 26°C, and 34°C). Fig. 6 *A* shows representative line-scan images of AQP4-EGFP-HeLa S3 cells and EGFP-HeLa S3 cells. Arrhenius plots showed that the activation energies of the AQP4-EGFP-HeLa S3 cells (high expression) and the control EGFP-HeLa S3 cells were 1.8 kcal/mol and 14.7 kcal/mol, respectively (Fig. 6 *B*). We also found that the activation energy was dependent on the expression levels of AQP4 at the cell membranes. In view of these findings, we concluded that CARS microscopy is a powerful method for measuring the water permeability of single cells and that it is sufficiently sensitive to distinguish AQP-mediated facilitated diffusion and the simple diffusion of water through cell membranes.

DISCUSSION

Here, we report an advanced method for visualizing H_2O or D_2O molecules directly based on CARS microscopy, which allows us to measure the kinetics of H_2O transport in single mammalian cells. Using this method, we distinguished the difference between simple diffusion and facilitated diffusion via AQP4. We found a positive correlation between AQP4 expression at the plasma membranes and the time constant for diffusional water permeability (P_d). The activation energy for AQP4-mediated water transport was also dependent on the expression levels of AQP4, but was significantly higher than that for diffusion through a lipid bilayer of the cell membranes.

We have made the following technical improvements for measuring the rapid exchange of H_2O/D_2O through mammalian cell membranes. First, we constructed a CARS microscope setup with a high-repetition-rate (76 MHz) pulsed laser source to ensure a sufficient signal/noise ratio. In our experiment, the pixel dwell time was set at 0.5 μs/pixel for a round-trip line-scanning mode to improve the temporal resolution by exposing 40 pulses to each pixel. In the experimental study of Potma et al., the repetition rate of the pulsed laser source was 800 kHz (15). Accordingly, the total number of pulses exposed to each pixel in their

experimental setup would be 0.4, if we applied the scanning mode used in this study. This calculation indicates that our CARS signal is 100 times more concentrated at each pixel. Second, we removed the external solution quickly enough to observe the efflux of H_2O from single HeLa S3 cells using CARS microscopy. Our τ_{CARS} for the external solution exchange was ~16.1 ms, whereas the exchange speed was ~1.5 s for the imaging of water transport in the microorganism *D. discoideum* (15). The exchange rate is therefore at least 90-fold faster in our setup. This quick exchange is important for observing the transport of H_2O in mammalian cells, because the efflux of H_2O from HeLa S3 cells, for example, ends within 1 s. Third, by using reinforced glass-bottomed dishes, our measurements can completely avoid defocusing during flushing (Fig. 1 *B*, *b* and *c*). We suspect that the main cause of defocusing is the flexural deformation of the coverglass during D_2O/BSS flushing. Therefore, a portion of a coverglass adhered to a plastic dish was reinforced using a low-elastic-coefficient adhesive material. With this reinforced glass-bottomed dish, we confirmed that defocusing was completely avoided and that the CARS signal was detected without any disturbance during the measurement.

HeLa S3 cells expressing AQP4-EGFP had a higher P_d. In this study, the P_d for EGFP-transfected HeLa S3 cells at room temperature was $8.3 \pm 2.6 \times 10^{-4}$ cm/s. This value is comparable to the value obtained by Ye et al. using fluorescent methods (6.3×10^{-4} cm/s at 23°C), which indicates the P_d for artificial liposomes composed of phosphatidylcholine and cholesterol (17). This conclusion is reasonable, because native HeLa S3 cells do not have any water channels. The P_d values are dependent on the lipid condition measured using NMR, for example, the P_d for liposomes containing 1,2-dioleoyl-*sn*-glycero-3-phosphocholine is $1.22 \pm 0.21 \times 10^{-2}$ cm/s at 25°C, whereas the P_d for liposomes containing 1,2-didocosahexaenoyl-*sn*-glycero-3-phosphocholine is $6.62 \pm 1.89 \times 10^{-2}$ cm/s at 25°C (10). The P_d for AQP4-EGFP-HeLa S3 cells is $2.7 \pm 1.0 \times 10^{-3}$ cm/s, which is ~3.3-fold larger than that for EGFP-HeLa S3 cells. This increase is consistent with the results reported by Ye et al. using a fluorescent method, which showed a 1.8-fold increase for ghost red blood cells with ($2.8 \pm 0.4 \times 10^{-3}$ cm/s) or without $HgCl_2$ ($5.1 \pm 0.5 \times 10^{-3}$ cm/s) (17). We suspect that the slight difference in the absolute P_d values for AQP4-EGFP-HeLa S3 cells and human erythrocytes or ghost red blood cells is due to differences in expression levels and lipid conditions (10,17,18).

Arrhenius plots showed a low activation energy for AQP4-EGFP-HeLa S3 cells, indicating that AQP4 is the main pathway for water transport. Note that the activation energy for AQP4-EGFP-HeLa S3 cells was similar to that for ghost or human erythrocytes, which express high copy numbers of AQP1 (17,18). In control HeLa S3 cells, water mainly permeates through the lipid bilayer of the membranes, because lipid fluidity can be affected by temperature. Therefore, the activation energy for the control HeLa S3 cells was high (14.7 kcal/mol), similar to those for liposomes or human erythrocytes after AQP1 inhibition by mercury (17,18). These results indicate that our CARS microscopy method using a quick flushing device may be useful for evaluating the diffusion of water in single mammalian cells.

By monitoring the fluorescence intensity of AQP4-EGFP at the plasma membrane of the transfected cells, we found a positive correlation between AQP4 expression and the P_d of the membrane. The membrane transport of AQP4 is regulated by phosphorylation in vitro (19). It has been demonstrated that the expression level of AQP4 in astrocytes changes during brain edema formation (20). The function of AQP4 is inhibited by metal ions, as well as some chemical compounds (21). It is therefore worth using our CARS microscopy to study the dynamic regulation of AQP during certain physiological and pathological conditions.

SUPPORTING MATERIAL

A movie is available at http://www.biophysj.org/biophysj/supplemental/S0006-3495(11)01021-6.

This work was supported by Molecular Ensemble Research at RIKEN (A.M.), Human Frontier Science Program (A.M.), Global Center of Excellence Program for Humanoid Metabolomic Systems Biology of the Ministry of Education, Culture, Sports, Science and Technology (MEXT) of Japan (T.M. and M.Y.), the Japan New Energy and Industrial Technology Development Organization (NEDO) (M.Y.) and Keio University Program for the Advancement of Next Generation Research Projects (M.Y.).

REFERENCES

1. Finkelstein, A. 1987. Water Movement through Lipid Bilayers, Pores, Plasma Membranes: Theory and Reality. John Wiley and Sons, New York.

2. Blok, M. C., L. L. M. Van Deenen, and J. De Gier. 1977. The effect of cholesterol incorporation on the temperature dependence of water permeation through liposomal membranes prepared from phosphatidylcholines. *Biochim. Biophys. Acta.* 464:509–518.

3. Zeidel, M. L., S. V. Ambudkar, …, P. Agre. 1992. Reconstitution of functional water channels in liposomes containing purified red cell CHIP28 protein. *Biochemistry.* 31:7436–7440.

4. King, L. S., D. Kozono, and P. Agre. 2004. From structure to disease: the evolving tale of aquaporin biology. *Nat. Rev. Mol. Cell Biol.* 5: 687–698.

5. Deen, P. M., M. A. Verdijk, …, B. A. van Oost. 1994. Requirement of human renal water channel aquaporin-2 for vasopressin-dependent concentration of urine. *Science.* 264:92–95.

6. Francis, P., J. J. Chung, …, P. Agre. 2000. Functional impairment of lens aquaporin in two families with dominantly inherited cataracts. *Hum. Mol. Genet.* 9:2329–2334.

7. Murata, K., K. Mitsuoka, …, Y. Fujiyoshi. 2000. Structural determinants of water permeation through aquaporin-1. *Nature.* 407:599–605.

8. de Groot, B. L., and H. Grubmüller. 2001. Water permeation across biological membranes: mechanism and dynamics of aquaporin-1 and GlpF. *Science.* 294:2353–2357.

9. Preston, G. M., T. P. Carroll, …, P. Agre. 1992. Appearance of water channels in *Xenopus* oocytes expressing red cell CHIP28 protein. *Science.* 256:385–387.

10. Huster, D., A. J. Jin, …, K. Gawrisch. 1997. Water permeability of polyunsaturated lipid membranes measured by ^{17}O NMR. *Biophys. J.* 73:855–864.

11. Fabry, M. E., and M. Eisenstadt. 1975. Water exchange between red cells and plasma. Measurement by nuclear magnetic relaxation. *Biophys. J.* 15:1101–1110.

12. Verkman, A. S., and K. R. Wong. 1987. Proton nuclear magnetic resonance measurement of diffusional water permeability in suspended renal proximal tubules. *Biophys. J.* 51:717–723.

13. Wong, K. R., and A. S. Verkman. 1987. Human platelet diffusional water permeability measured by nuclear magnetic resonance. *Am. J. Physiol.* 252:C618–C622.

14. Kuwahara, M., and A. S. Verkman. 1988. Direct fluorescence measurement of diffusional water permeability in the vasopressin-sensitive kidney collecting tubule. *Biophys. J.* 54:587–593.

15. Potma, E., W. P. de Boeij, …, D. A. Wiersma. 2001. Real-time visualization of intracellular hydrodynamics in single living cells. *Proc. Natl. Acad. Sci. USA.* 98:1577–1582.

16. Cheng, J. X., A. Volkmer, and X. S. Xie. 2002. Theoretical and experimental characterization of coherent anti-Stokes Raman scattering microscopy. *J. Opt. Soc. Am. B.* 19:1363–1375.

17. Ye, R. G., and A. S. Verkman. 1989. Simultaneous optical measurement of osmotic and diffusional water permeability in cells and liposomes. *Biochemistry.* 28:824–829.

18. Fettiplace, R., and D. A. Haydon. 1980. Water permeability of lipid membranes. *Physiol. Rev.* 60:510–550.

19. Kadohira, I., Y. Abe, …, M. Yasui. 2008. Phosphorylation in the C-terminal domain of Aquaporin-4 is required for Golgi transition in primary cultured astrocytes. *Biochem. Biophys. Res. Commun.* 377:463–468.

20. Vizuete, M. L., J. L. Venero, …, J. Cano. 1999. Differential upregulation of aquaporin-4 mRNA expression in reactive astrocytes after brain injury: potential role in brain edema. *Neurobiol. Dis.* 6:245–258.

21. Yukutake, Y., Y. Hirano, …, M. Yasui. 2009. Rapid and reversible inhibition of aquaporin-4 by zinc. *Biochemistry.* 48:12059–12061.